

Electrochemical Template Synthesis of Multisegment Nanowires: Fabrication and Protein Functionalization[†]

Bridget Wildt,^{‡,||} Prashant Mali,^{§,||} and Peter C. Searson^{*,‡}

Department of Materials Science and Engineering and Institute for NanoBioTechnology and The Whitaker Biomedical Engineering Institute, Johns Hopkins University, Baltimore, Maryland 21218

Received April 29, 2006. In Final Form: July 21, 2006

Multisegment nanowires represent a unique platform for engineering multifunctional nanoparticles for a wide range of applications. For example, the optical and magnetic properties of nanowires can be tailored by modifying the size, shape, and composition of each segment. Similarly, surface modification can be used to tailor chemical and biological properties. In this article, we report on recent work on electrochemical template synthesis of nanogap electrodes, the fabrication of multisegment nanowires with embedded catalysts, and the selective functionalization of multisegment nanowires with proteins.

Introduction

From an engineering perspective, the properties of nanoparticles can be designed for specific applications by taking advantage of the degrees of freedom associated with the system. For example, physical characteristics such as the size, shape, and composition can be used to tailor the electrical, optical, and magnetic properties.^{1–8} Chemical modification can be used to tailor surface properties (hydrophilicity or hydrophobicity, surface charge, etc), impart other properties (e.g., fluorescence), and introduce molecular recognition for small molecules (e.g., drugs), biopolymers (e.g., peptides, proteins, and DNA), protein assemblies (e.g., viruses), and other nanoparticles (e.g., particle–DNA conjugates).^{9–14}

The ability to control these parameters is largely dependent on the synthesis or fabrication technique. Electrochemical template synthesis allows the fabrication of single-component and multisegment nanowires with diameters as small as a few nanometers.^{15,16} This technique has the ability to introduce

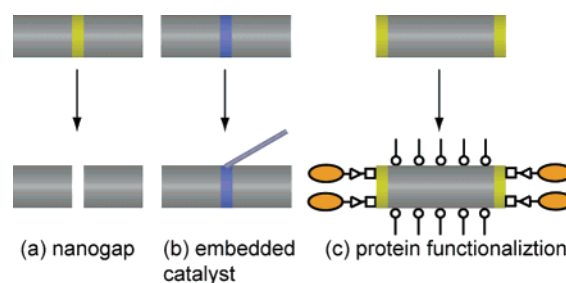


Figure 1. Schematic illustration of (a) the formation of nanogaps, (b) multisegment nanowires with embedded catalysts, and (c) selective protein functionalization of multisegment nanowires.

different segments along the length of the nanowire and is particularly attractive in designing particles with complex functions.^{5,12,13,17–22} Individual segments may include metals, alloys, metal oxides, or electronically conducting polymers and hence can introduce specific magnetic, optical, or electrical properties. Surface functionalization can be achieved by coating the nanowires (e.g. with fibronectin to promote cell adhesion) or through a molecular linkage (e.g. thiol on a gold segment). Using molecular linkages that bind specifically to different materials enables spatially localized surface functionalization to be achieved. Attaching proteins to individual segments of nanowires to achieve differential functionalization is particularly challenging because proteins tend to bind to most surfaces.

In this article, we report on our recent work on electrochemical template synthesis of multisegment nanowires and selective functionalization with proteins. We discuss two examples of novel nanowire architectures: nanogap electrodes and multisegment nanowires with embedded catalysts (Figure 1). Surface

[†] Part of the Electrochemistry special issue.

^{*} To whom correspondence should be addressed. E-mail: searson@jhu.edu.

[‡] Department of Materials Science and Engineering and Institute for NanoBioTechnology.

[§] The Whitaker Biomedical Engineering Institute.

^{||} Both authors contributed equally.

(1) Sun, L.; Hao, Y.; Chien, C. L.; Searson, P. C. *IBM J. Res. Dev.* **2005**, *49*, 79–102.

(2) Sellmyer, D. J.; Zheng, M.; Skomski, R. *J. Phys.: Condens. Matter* **2001**, *13*, R433–R460.

(3) Kovtyukhova, N. I.; Mallouk, T. E. *Chem.—Eur. J.* **2002**, *8*, 4355–4363.

(4) Ji, C.; Searson, P. C. *J. Phys. Chem. B* **2003**, *107*, 4494–4499.

(5) Nicewarner-Pena, S. R.; Freeman, R. G.; Reiss, B. D.; He, L.; Pena, D. J.; Walton, I. D.; Cromer, R.; Keating, C. D.; Natan, M. J. *Science* **2001**, *294*, 137–141.

(6) Park, S.; Chung, S. W.; Mirkin, C. A. *J. Am. Chem. Soc.* **2004**, *126*, 11772–11773.

(7) Zhang, Y.; Kolmakov, A.; Chretien, S.; Metiu, H.; Moskovits, M. *Nano Lett.* **2004**, *4*, 403–407.

(8) Sun, L.; Searson, P. C.; Chien, C. L. *Phys. Rev. B* **2000**, *61*, R6463–R6466.

(9) Martin, B. R.; Dermody, D. J.; Reiss, B. D.; Fang, M. M.; Lyon, L. A.; Natan, M. J.; Mallouk, T. E. *Adv. Mater.* **1999**, *11*, 1021–1025.

(10) Tanase, M.; Bauer, L. A.; Hultgren, A.; Silevitch, D. M.; Sun, L.; Reich, D. H.; Searson, P. C.; Meyer, G. J. *Nano Lett.* **2001**, *1*, 155–158.

(11) Bauer, L. A.; Reich, D. H.; Meyer, G. J. *Langmuir* **2003**, *19*, 7043–7048.

(12) Salem, A. K.; Searson, P. C.; Leong, K. W. *Nat. Mater.* **2003**, *2*, 668–671.

(13) Chen, M.; Guo, L.; Ravi, R.; Searson, P. C. *J. Phys. Chem. B* **2006**, *110*, 211–217.

(14) Cui, Y.; Wei, Q. Q.; Park, H. K.; Lieber, C. M. *Science* **2001**, *293*, 1289–1292.

(15) Possin, G. E. *Rev. Sci. Instrum.* **1970**, *41*, 772–774.

(16) Martin, C. R. *Science* **1994**, *266*, 1961–1966.

(17) Piraux, L.; George, J. M.; Despres, J. F.; Leroy, C.; Ferain, E.; Legras, R.; Ounadjela, K.; Fert, A. *Appl. Phys. Lett.* **1994**, *65*, 2484–2486.

(18) Blondel, A.; Meier, J. P.; Doudin, B.; Ansermet, J. P. *Appl. Phys. Lett.* **1994**, *65*, 3019–3021.

(19) Liu, K.; Nagodawithana, K.; Searson, P. C.; Chien, C. L. *Phys. Rev. B* **1995**, *51*, 7381–7384.

(20) Chen, M.; Chien, C. L.; Searson, P. C. *Chem. Mater.* **2006**, *18*, 1595–1601.

(21) Park, S.; Lim, J. H.; Chung, S. W.; Mirkin, C. A. *Science* **2004**, *303*, 348–351.

(22) Paxton, W. F.; Kistler, K. C.; Olmeda, C. C.; Sen, A.; St Angelo, S. K.; Cao, Y. Y.; Mallouk, T. E.; Lammert, P. E.; Crespi, V. H. *J. Am. Chem. Soc.* **2004**, *126*, 13424–13431.

functionalization of nanoparticles is of increasing interest in nanobiotechnology, and we present four strategies for achieving spatially selective protein functionalization of multisegment nanowires (Figure 1). These schemes provide examples of approaches that can be adapted to a wide range of proteins and nanowire segments.

Experimental Section

Nanogap Fabrication. Au/Ni/Au nanowires were deposited in alumina templates with 200-nm-diameter pores (Whatman). A 750-nm-thick copper layer was thermally evaporated onto the branched side of the template. Templates were immersed in DI water and then assembled into a Teflon cell with an exposed area of 0.785 cm². In the first step, copper was deposited into the branched region of the template at -0.16 V (Ag/AgCl) (5 C cm⁻²) from 0.5 M CuSO₄ (pH 1.0, adjusted using H₂SO₄). Au segments (6 μm long) were deposited from a commercial solution (Technic 434) at -0.127 mA cm⁻² (51% efficiency). Next, 10 – 500 -nm-long Ni segments were deposited from solution containing 0.5 M NiSO₄ (Sigma-Aldrich) and 0.67 M H₃BO₃ (J. T. Baker) at -0.127 mA cm⁻² (39% efficiency). Finally, another 6 -μm-long Au segment was deposited. Care was taken to rinse the template thoroughly between each step to prevent contamination from ions present in the previous step.

The copper layer on the back side of the template was removed by etching in 10 g of CuCl₂ (Alfa Aesar), 10 mL of HCl (Fischer), and 250 mL of DI water for 1 h. Templates were then washed in DI water and dissolved in 2 M KOH for 2.5 h at 75 °C. After this step, while still in KOH, the wires were sonicated for about 10 min and allowed to settle under gravity and were then washed in ethanol several times. Centrifugation was avoided at all steps to prevent these relatively long (12 μm) wires from bending. The wires were finally stored in 10 mL of ethanol to a final concentration of the order of 10^7 mL⁻¹.

A dilute suspension of the nanowires was dispersed on thermally oxidized silicon wafers (500 nm SiO₂ thickness). Photolithography was used to pattern 300 nm thick Au contact electrodes over the ends of the wire. Finally, the nickel segments were etched in 25% HNO₃ (EMD) for 60 min. The nanowires were then washed sequentially in DI water, ethanol, and then allowed to dry in air.

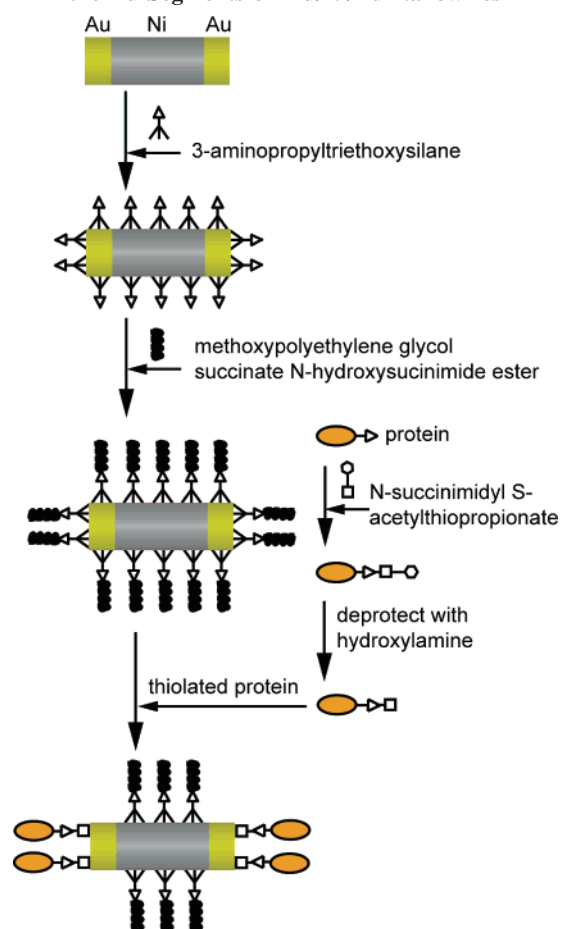
Nanowires with Embedded Catalysts. Multisegment Pt/Co nanowires were deposited from solution containing 0.01 M K₂PtCl₆ (Alfa Aesar), 0.1 M CoSO₄ (Alfa Aesar), and 0.5 M H₃BO₃. The Pt segments were deposited at -0.1 V (Ag/AgCl), and the Co segments, at -0.95 V (Ag/AgCl). All other steps are as reported above, with the exception that the etching of the backside copper was restricted to 15 min, and the alumina template was dissolved at room temperature in 1 M NaOH for only 1 h. These modifications were used to minimize dissolution of the Co segments.

Carbon nanotube growth was carried out in a quartz tube furnace. The Pt/Co nanowires were dispersed on SiO₂ wafers and placed in alumina boats at 800 °C under 600 mL min⁻¹ CH₄ flow at 20 psi for 10 min with a 1000 mL min⁻¹ inert Ar flush during ramp up and ramp down. The ramp-up time (from room temperature) was about 11 min, and the ramp-down time (from 800 °C) was usually about 2.5 h.

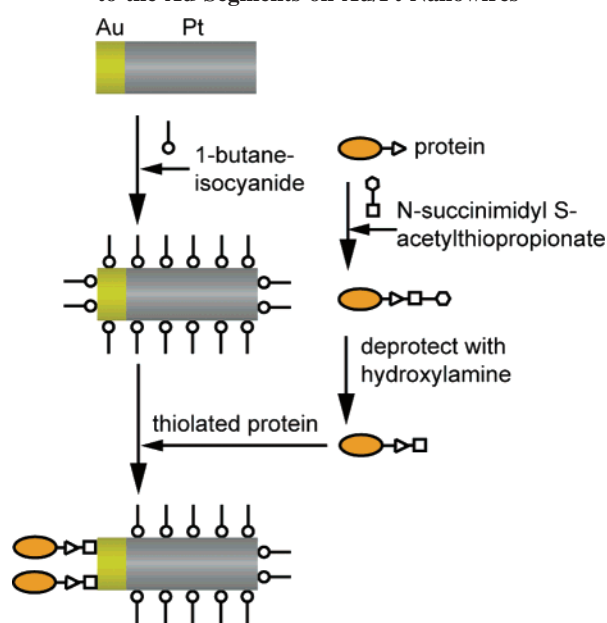
Nanowire Synthesis for Protein Functionalization. All Au segments were deposited at -0.9 V (Ag/AgCl) from a commercially available solution (Technic 434 HS), and Pt segments were deposited at -0.15 V (Ag/AgCl) from commercially available solution (Technic TP RTU) or solution containing 17 mM (NH₄)₂PtCl₆ (Aldrich) and 250 mM Na₂HPO₄ (Aldrich).²³ Ni segments were deposited at -1.0 V (Ag/AgCl) from 0.5 M NiSO₄ and 0.25 M H₃BO₃.

Protein Functionalization Schemes. Two proteins were used in this study: KE2 human HLA primary antibody and ActA. The proteins were fluorescently imaged in the following way. The KE2 human HLA antibody was visualized by adding a secondary

Scheme 1. Thiolated KE2 Antibody Selectively Bound to the Au Segments on Au/Ni/Au Nanowires

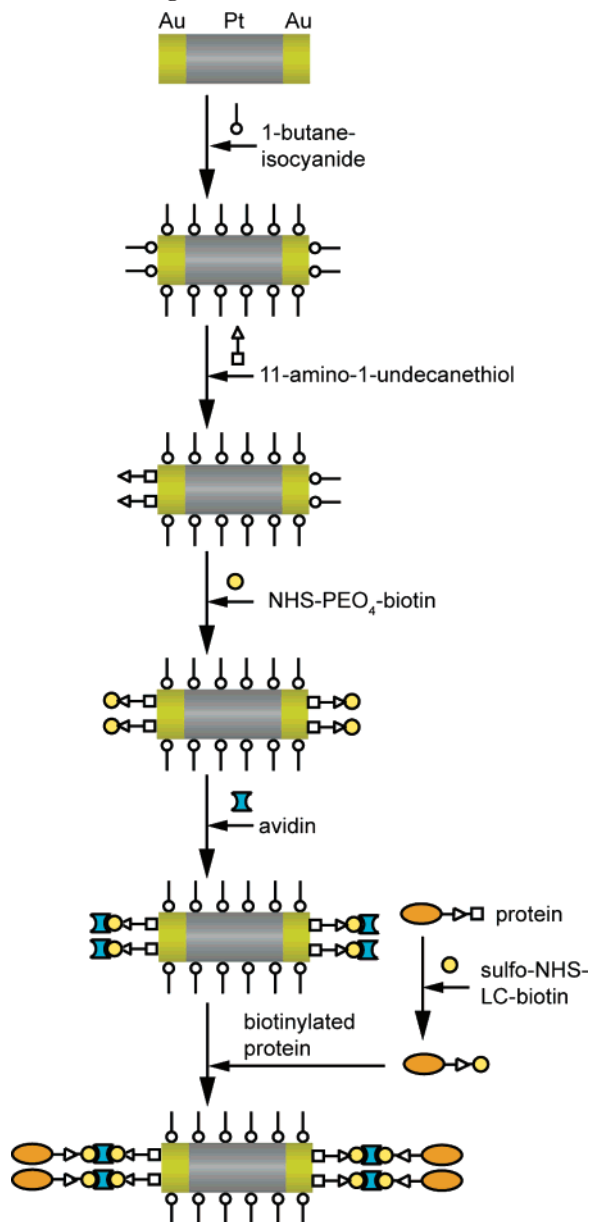


Scheme 2. Thiolated ActA-NH₂ Protein Selectively Bound to the Au Segments on Au/Pt Nanowires



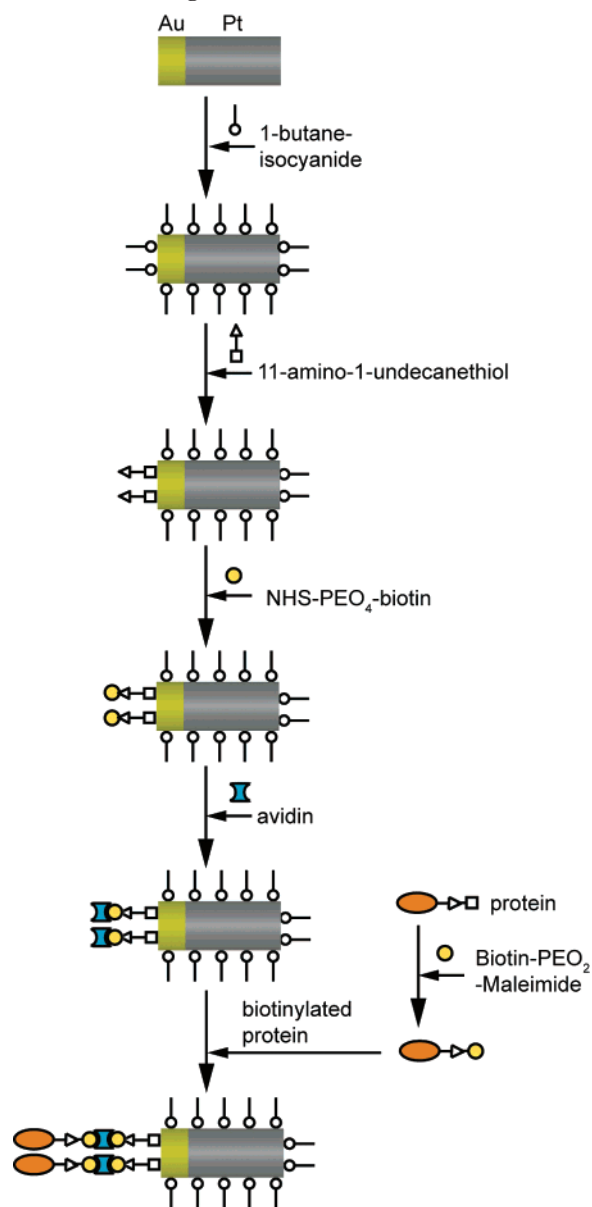
antibody—Alexa Fluor 488 goat antimouse IgG (Molecular Probes, excitation 488 nm). In Schemes 2 and 3, ActA was visualized through a fluorescein (fluorescein-5-maleimide, Molecular Probes) bound to a terminal cysteine residue on the ActA protein. In Scheme 4, the ActA protein was visualized through a fluorescein (fluorescein-5-Ex, succinimidyl ester, Molecular Probes) bound to primary amines on the surface lysine residues.

(23) Whalen, J. J.; Weiland, J. D.; Searson, P. C. *J. Electrochem. Soc.* **2005**, *152*, C738–C743.

Scheme 3. Biotinylated ActA-NH₂ Selectively Bound to the Au Segments on Au/Pt/Au Nanowires

The proteins were first removed from storage at -80 or -20 °C and centrifuged for 1 h at 100 000 rpm to remove any aggregates caused by freezing. The concentrations of the proteins were approximately 0.6 mg mL⁻¹ for ActA and 1.4 mg mL⁻¹ for KE2 human HLA primary antibody.

The KE2 human HLA primary antibody and ActA proteins in Schemes 1 and 2 were thiolated by adding 10 μ L of 63 mM *N*-succinimidyl-*S*-acetylthioacetate (SATP, Pierce) in dimethyl sulfoxide (DMSO, Alfa Aesar) to 1 mL of protein. The succinimide (NHS) group is coupled to primary amines on the protein (ActA-NH₂). The solution was vortexed and incubated at room temperature for 30 min. Excess reagent was removed by centrifuging in a 10 000 MW centrifugal filter device (Amicon Ultra-4, Millipore) at 3220 rpm for 20 min. The protein was further washed with 1 mL of phosphate-buffered saline (PBS, pH 7.4). The protein was resuspended in 1 mL of PBS by repipetting. At this point, the protein could be stored at -20 °C as the sulfhydryl group is protected. The sulfhydryl group is made available for reaction through deacetylation. Deacetylation was performed by combining the protein solution with 100 μ L of 25 mM ethylenediaminetetraacetic acid (EDTA, Baker) and 500 mM hydroxylamine (Pierce). The solution was vortexed and incubated for 2 h at room temperature. Then the solution

Scheme 4. Biotinylated ActA-Cys Selectively Bound to the Au Segments on Au/Pt Nanowires

was desalted as before with 1 mL of PBS containing 100 mM EDTA. Finally, the protein was resuspended in PBS.

ActA in Scheme 3 was biotinylated by reacting 10 mM sulfo-succinimidyl-6-(biotin-amido)hexanoate (sulfo-NHS-LC-biotin, Pierce) with 500 μ L of ActA protein. As in Schemes 1 and 2, the succinimide (NHS) group is coupled to primary amines on the protein (ActA-NH₂). The solution was then mixed and incubated for 30 min at room temperature. Excess reagent was removed as before, and the protein was resuspended in PBS.

ActA in Scheme 4 was biotinylated through a terminal cysteine residue (ActA-Cys) by reacting 100 μ L of 19 mM biotinyl-3-maleimidopropionamidyl-3,6-dioxaoctanediamine (maleimide-PEO₂-biotin, Pierce) in PBS (phosphate buffered saline, 7.4) with 200 μ L ActA protein. The solution was then mixed and incubated for 2 h at room temperature. Excess reagent was removed as described above, and the protein was resuspended in PBS.

Prior to functionalization, the nanowires were removed from the template, suspended, and washed in ethanol at least twice. Nanowires with Ni segments were collected using a magnet; nanowires without a Ni segment were collected by centrifugation at 3000 rpm for 10 min. The number of nanowires in each experiment was approximately 5×10^7 . All light microscope and fluorescence images were obtained

using a Nikon TE2000U inverted microscope and IPLab software. All fluorescence images are the raw images; no image modification was used.

Multisegment Au/Ni/Aunanowires with $1\ \mu\text{m}$ ($0.81\ \text{C cm}^{-2}$) Au segments and a $5.5\ \mu\text{m}$ ($7.1\ \text{C cm}^{-2}$) Ni segment were deposited at constant potential. After washing, the nanowires were suspended in $500\ \mu\text{L}$ of $10\ \text{mM}$ (3-aminopropyl)triethoxysilane (Aldrich) in ethanol, sonicated briefly, and vortexed overnight in a plastic Eppendorf tube. The nanowires were then washed with $500\ \mu\text{L}$ of ethanol (ACS/USP, Pharmco) and sonicated at least three times. The nanowires were washed twice with $500\ \mu\text{L}$ of $0.1\ \text{M}$ sodium bicarbonate (Aldrich). Methoxypoly(ethylene glycol) succinate *N*-hydroxysuccinimide ester (PEG, $0.1\ \text{mg}$, Aldrich) and $500\ \mu\text{L}$ of $0.1\ \text{M}$ sodium bicarbonate were added to the nanowire suspension, sonicated briefly, and vortexed for $1\ \text{h}$. The wires were then washed as before with sodium bicarbonate, suspended in the thiolated protein solution, vortexed for about $20\ \text{min}$, and incubated overnight at $4\ ^\circ\text{C}$ on an end-to-end mixer. The nanowires were washed twice with PBS, and then $500\ \mu\text{L}$ of secondary antibody (diluted 1:200 with PBS) was added to the vial, vortexed, and rotated gently at room temperature for $30\ \text{min}$. The nanowires were then washed with PBS at least three times.

Multisegment Au/Pt nanowires with a $2.5\ \mu\text{m}$ ($2.1\ \text{C cm}^{-2}$) Au segment and a $4.5\ \mu\text{m}$ ($8.4\ \text{C cm}^{-2}$) Pt segment were deposited at constant potential. After washing, the nanowires were treated with $1\ \text{mL}$ of $4\ \text{mM}$ butyl isocyanide (BIC, Aldrich) in dimethylformide (DMF, Alfa Aesar), sonicated briefly, and vortexed overnight. The nanowires were then washed with DI water, sonicated, and vortexed at least three times. At least $300\ \mu\text{L}$ of thiolated ActA protein was added to the nanowires immediately after deacetylation, and they were vortexed for about $30\ \text{min}$. The wires were incubated overnight at $4\ ^\circ\text{C}$ and washed in ActA buffer at least three times before imaging.

Au/Pt/Au nanowires with $1\ \mu\text{m}$ Au segments ($0.81\ \text{C cm}^{-2}$) and a $6\ \mu\text{m}$ ($10\ \text{C cm}^{-2}$) Pt segment were deposited at constant potential. The nanowires were treated with BIC and 11-amino-1-undecanethiol (Scheme 3) and washed as before, and $500\ \mu\text{L}$ of $4\ \text{mM}$ NHS-PEO₄-biotin (Pierce) in PBS was added to the nanowires, which were vortexed for $2\ \text{h}$. After washing, $0.05\ \text{mg mL}^{-1}$ NeutrAvidin (NATR, Pierce) was added to the suspension and reacted with intermittent vortexing for $30\ \text{min}$. The nanowires were washed in PBS three times, and $500\ \mu\text{L}$ of biotinylated ActA was added to the nanowires with vortexing for $30\ \text{min}$. The nanowires were washed in PBS with brief sonication and vortexing.

Au/Pt nanowires with $4.0\ \mu\text{m}$ ($3.2\ \text{C cm}^{-2}$) Au and $6.0\ \mu\text{m}$ ($8.1\ \text{C cm}^{-2}$) Pt segments were deposited at constant potential. The platinum segment was functionalized with BIC as described in Scheme 2. After washing, $500\ \mu\text{L}$ of 1 to $2\ \text{mM}$ 11-amino-1-undecanethiol (Dojindo) in DMSO was added, and the wires were vortexed for $2\ \text{h}$. The wires were washed in DMSO with sonication at least three times. NHS-PEO₄-biotin ($500\ \mu\text{L}$, $4\ \text{mM}$, Pierce) in DMF and $10\ \mu\text{L}$ of concentrated triethylamine (Alfa Aesar) were added to the wires and vortexed for $2\ \text{h}$. The nanowires were washed with DMF, and then $0.05\ \text{mg mL}^{-1}$ NeutrAvidin (NATR, Pierce) was added to the suspension and reacted with intermittent vortexing for $30\ \text{min}$. The nanowires were washed in PBS three times, and then the biotinylated ActA-Cys was added. The wires were vortexed for $30\ \text{min}$ and incubated overnight at $4\ ^\circ\text{C}$. The wires were then washed at least three times with PBS.

Results and Discussion

Fabrication of Nanogap Electrodes. Nanogaps are used as building blocks for quantum devices and for studying electron transport in small molecules and proteins.^{24–26} Recently, it has been demonstrated that nanogaps can be formed using electro-

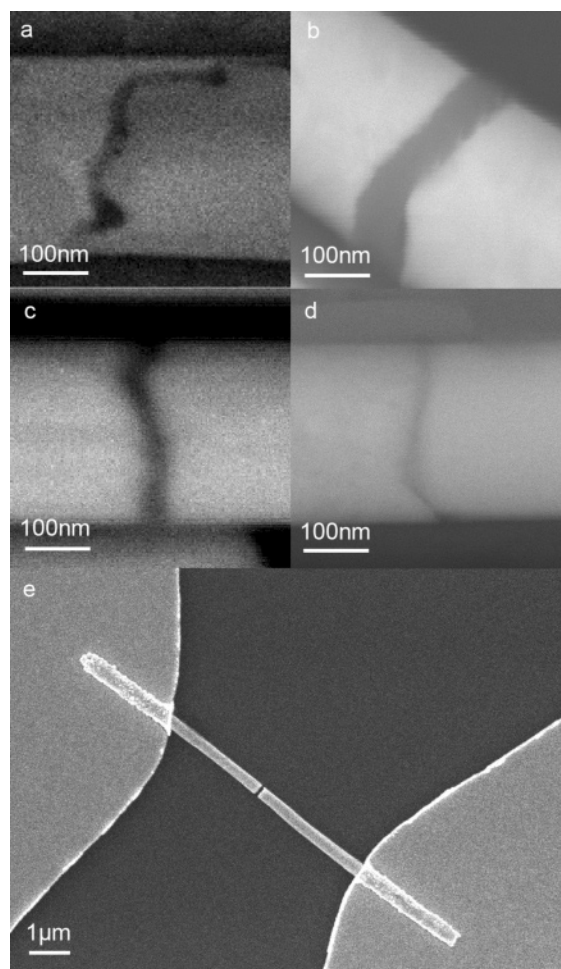


Figure 2. SEM image of a Au/Ni/Au nanowire where the Au and Ni segments were deposited at (a) $-1\ \text{V}$ (Ag/AgCl) and (b) $-0.127\ \text{mA cm}^{-2}$. SEM images of a Au nanowire with (c) $25\ \text{nm}$ and (d) $10\ \text{nm}$ nanogaps formed by etching the Ni segment. (e) SEM image of a $100\ \text{nm}$ nanogap device.

chemical template synthesis.^{27,28} Below we outline our fabrication procedure and discuss some of the underlying engineering issues associated with this technique.

Briefly, we first electrodeposit Au/Ni/Au nanowires with sacrificial Ni segments varying from 10 to $500\ \text{nm}$ in length. Next, the nanowires are dispersed onto an insulating substrate, and gold pads deposited onto the ends of the wires using projection photolithography. Importantly, these pads also serve to fix the nanowires onto the substrate. Liu et al.²⁷ used thermal decomposition of a surfactant layer on the gold segments to bind the Au/Ag/Au nanowires to the substrate, whereas Qin et al.²⁸ used a SiO_2 film on the Au/Ni/Au nanowires to hold the Au segments together after etching. Finally, the Ni segment is etched in nitric acid for $60\ \text{min}$ to yield electrodes with a nanogap with dimensions corresponding to the length of the Ni segment.

A critical issue in the synthesis of nanogaps is the reproducible and conformal deposition of the individual nanowire segments. Deposition of Ni and Au segments under typical electrodeposition conditions (about $-1.0\ \text{V}$ (Ag/AgCl)) yields rough interfaces and segments of varying length with the gold segments on either side often penetrating across the nickel layer when the segment thickness is below $100\ \text{nm}$ (Figure 2a). Two factors were found to be helpful in producing uniform interfaces and reproducible

(24) Bezryadin, A.; Dekker, C.; Schmid, G. *Appl. Phys. Lett.* **1997**, *71*, 1273–1275.

(25) Morpurgo, A. F.; Marcus, C. M.; Robinson, D. B. *Appl. Phys. Lett.* **1999**, *74*, 2084–2086.

(26) Cheng, C. D.; Gonela, R. K.; Gu, Q.; Haynie, D. T. *Nano Lett.* **2005**, *5*, 175–178.

(27) Liu, S. H.; Tok, J. B. H.; Bao, Z. N. *Nano Lett.* **2005**, *5*, 1071–1076.

(28) Qin, L. D.; Park, S.; Huang, L.; Mirkin, C. A. *Science* **2005**, *309*, 113–115.

gap segments. First, the templates were extensively rinsed and immersed in the deposition solution for at least 30–60 min to ensure that all pores were uniformly wet. This resulted in constant deposition efficiency from batch to batch. Second, deposition was carried out relatively slowly (typically -0.096 to -0.127 mA cm $^{-2}$ or at -0.9 V (Ag/AgCl) for Au and -0.8 V (Ag/AgCl) for Ni). At -0.1 mA cm $^{-2}$, reproducible nickel segments as short as 10 nm (i.e., a 1/30 aspect ratio for the 300-nm-diameter nanowires) were obtained (Figure 2b–d). Using this technique, we found that the two interfaces of the central segment were nearly parallel and the interface roughness was reduced to below 5 nm.

In fabricating nanogap devices, residual organic impurities on the gold segments during the intermediate lithographic processes often result in poor electrical contacts. Care has to be taken to ensure that the resist is fully developed and subsequently etched at each step. Also, a brief oxygen plasma exposure before evaporation of the contact pads ensures good electrical contacts. Finally, for mechanical stability the contact pad thickness was at least twice the radius of the nanowires to ensure that shadow masking did not prevent complete end-coating of the nanowires. Figure 2e shows a 100 nm nanogap device.

Embedded Catalyst Pt/Co Multisegment Nanowires. Multisegment nanowires provide a powerful tool for exploiting differences in optical reflectivity or magnetic properties of different materials. An area that has not been widely studied is the introduction of catalytic segments for the synthesis of carbon nanotubes, semiconductor nanowires, and other organic/inorganic nanowires through processes such as chemical vapor deposition²⁹ or solution–liquid–solid techniques.³⁰ Here we demonstrate the fabrication of multisegment Pt/Co nanowires. Co is a catalyst for carbon nanotubes and many semiconductor nanowires. Pt is chemically inert and has a melting point of 1772 °C, which is higher than the melting temperature of Co (1495 °C) and hence is preferable to Au, which has a melting temperature of 1064 °C.

In some cases, electrodeposition of multisegment nanowires with two components can be achieved from a single solution containing the ions of two components. By modulation of the potential or current, multilayers of the form A_xB_{1-x}/A with $x < 0.10$ can be deposited by ensuring that the concentration of the more noble component is very low (i.e., $[A^{n+}] \ll [B^{m+}]$). In this case, the more noble component A (e.g., Pt) is deposited at positive potentials, and an A_xB_{1-x} alloy is deposited at more negative potentials. This approach has been successfully exploited in the deposition of multilayers with alternating ferromagnetic (FM) and nonmagnetic (NM) layers that exhibit giant magnetoresistance (GMR). Examples of FM/NM multilayer nanowires deposited from a single solution containing the ions of both components include Co/Cu,^{17–19} Ni/Cu,^{20,31,32} CoNi/Cu,^{18,33} NiFe/Cu,^{34–36} and Ag/Au.³⁷

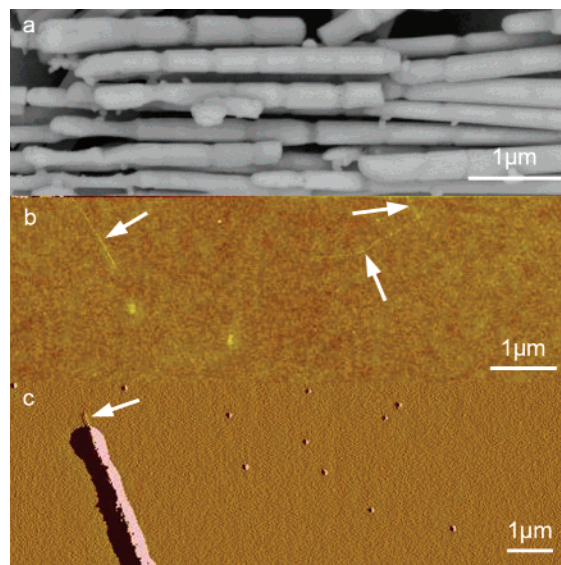


Figure 3. (a) SEM image of Pt/Co multisegment nanowires. Note that the Co segments are slightly etched during the extraction procedure. (b) AFM image showing SWNTs (1.4 nm diameter) grown on Co thin films on SiO₂. (c) AFM image of a SWNT (1.4 nm diameter) growing from the Co end-segment of a Co/Pt nanowire.

Figure 3a shows Pt/Co multisegment nanowires deposited from a single solution by modulating the deposition potential. We note that the template used for deposition imposes some constraints on the deposition solution; the alumina templates used here are stable only at intermediate pH.

In preliminary experiments, we have grown short single-walled carbon nanotubes on Co/Pt nanowires. Figure 3c shows an AFM image of a short single-walled carbon nanotube grown at the Co end-segment of a Co/Pt nanowire. Figure 3b shows carbon nanotubes grown under identical conditions on a thin 2.5 nm Co film. In both cases, the height is measured as 1.4 nm along the entire length, as expected for single-walled carbon nanotubes. These preliminary experiments suggest that the embedded catalyst approach can be used for the synthesis of a wide range of carbon and semiconductor nanowires.

Surface Functionalization. Functionalizing surfaces with chemical or biological groups has become an important tool in nanobiotechnology. Multisegment nanowires allow multiple chemical functionality to be introduced by exploiting the different affinities of functional groups (e.g., thiols, isocyanides, carboxylates) for different materials. However, a major challenge associated with binding proteins and other biomolecules is achieving selective functionalization. Although self-assembled monolayers on planar surfaces are well characterized, the influence of nanowire geometry on monolayer formation is not known. For example, studies of thiol formation on gold nanoparticles have indicated that the molecular density increases in regions of high curvature whereas the density of tail groups is decreased compared to a flat surface.³⁸

When selectively functionalizing the surface of multisegment nanowires, the first consideration is selecting the coupling linkages and the corresponding segments. For example, thiols bind strongly to gold and silver, carboxylic acids and siloxanes bind selectively to the native oxide on transition metals such as nickel and cobalt, and isocyanides bind strongly to platinum and palladium. However, in achieving selective functionalization of multisegment

(29) Kong, J.; Soh, H. T.; Cassell, A. M.; Quate, C. F.; Dai, H. J. *Nature* **1998**, *395*, 878–881.

(30) Trentler, T. J.; Hickman, K. M.; Goel, S. C.; Viano, A. M.; Gibbons, P. C.; Buhro, W. E. *Science* **1995**, *270*, 1791–1794.

(31) Chen, M.; Sun, L.; Bonevich, J. E.; Reich, D. H.; Chien, C. L.; Searson, P. C. *Appl. Phys. Lett.* **2003**, *82*, 3310–3312.

(32) Wang, L.; Yu Zhang, K.; Metrot, A.; Bonhomme, P.; Troyon, M. *Thin Solid Films* **1996**, *288*, 86–89.

(33) Evans, P. R.; Yi, G.; Schwarzacher, W. *Appl. Phys. Lett.* **2000**, *76*, 481–483.

(34) Dubois, S.; Marchal, C.; Beuken, J. M.; Piriaux, L.; Duvail, J. L.; Fert, A.; George, J. M.; Maurice, J. L. *Appl. Phys. Lett.* **1997**, *70*, 396–398.

(35) Dubois, S.; Piriaux, L.; George, J. M.; Ounadjela, K.; Duvail, J. L.; Fert, A. *Phys. Rev. B* **1999**, *60*, 477–484.

(36) Maurice, J. L.; Imhoff, D.; Etienne, P.; Durand, O.; Dubois, S.; Piriaux, L.; George, J. M.; Galtier, P.; Fert, A. *J. Magn. Magn. Mater.* **1998**, *184*, 1–18.

(37) Ji, C. X.; Oskam, G.; Ding, Y.; Erlebacher, J. D.; Wagner, A. J.; Searson, P. C. *J. Electrochem. Soc.* **2003**, *150*, C523–C528.

(38) Hostetler, M. J.; Wingate, J. E.; Zhong, C. J.; Harris, J. E.; Vachet, R. W.; Clark, M. R.; Londono, J. D.; Green, S. J.; Stokes, J. J.; Wignall, G. D.; Glish, G. L.; Porter, M. D.; Evans, N. D.; Murray, R. W. *Langmuir* **1998**, *14*, 17–30.

nanowires, the relative binding affinities and the order of functionalization are critically important. Functionalizing with proteins and other biomolecules is further complicated by the fact that biomolecules, and particularly proteins, nonspecifically bind to most surfaces, especially surfaces that are ionic and hydrophobic. Therefore, the difficulty is in selectively removing the proteins or in making the surface selectively protein resistant.

Here we discuss four schemes for selectively functionalizing nanowires with proteins through the formation of strong covalent linkages. In Schemes 1 and 2, we use the coupling of primary amine groups to thiols as a method to attach a protein to Au segments. In Scheme 1, we use a Ni segment functionalized with PEG as the protein-resistant segment, and in Scheme 2, we use a Pt segment functionalized with short-chain isocyanide as the protein-resistant segment. In Schemes 3 and 4, we attach biotinylated proteins to the gold surface via a biotin–avidin complex. In Scheme 3, we use the succinimide coupling reaction to biotinylate primary amines along the protein sequence. Finally, in Scheme 4 we use maleimide coupling to cysteine residues to biotinylate the terminal cysteine residue on the protein.

In Scheme 1, a protein is bound selectively to the Au end-segments of Au/Ni/Au nanowires through a thiol linkage introduced into the protein. The nanowires are first exposed to an amine-terminated siloxane. The siloxane group has a very high affinity for the native oxide on the Ni segment and is nonspecifically bound to the Au end-segments. A poly(ethylene glycol) moiety is then bound to the amino terminus of the siloxane through an *N*-hydroxysuccinimide coupling reaction with the primary amine. The coupling is performed in sodium bicarbonate to maintain the pH between 7 and 9. The PEG termination provides a hydrophilic surface that minimizes protein adsorption.

In the next step, the nanowires were exposed to KE2 human HLA antibody. The protein was thiolated using the *N*-hydroxysuccinimide coupling reaction with the primary amines on the protein surface. The succinimide ester portion of the SATP reacts with unprotonated primary amines to form covalent amide bonds upon loss of the hydroxysuccinimide. In aqueous solutions, this reaction is in competition with hydrolysis, which becomes more favorable at higher pH. In this example, the antibody was reacted in PBS at pH 7.4 to reduce hydrolysis but still allow for a reasonable probability that some primary amines on the protein are unprotonated. Primary amines can be found on the *N*-terminal end of a protein (α amine) or the side chain of a lysine amino acid (ϵ amine). Taking the pK_a of an α amine as 7.8 and the pK_a of an ϵ amine as 10.1, the Henderson–Hasselback equation predicts that at pH 7.4 about 1 in every 2.5 α amines is unprotonated (40%) whereas 1 in every 502 ϵ amines is unprotonated.³⁹ Assuming that there are 4–6% lysine residues (a four-chain IgG molecule contains 1340 residues (450 heavy and 220 light), which gives about 50–80 lysines per IgG molecule), the probability of an unprotonated ϵ amine on a particular IgG molecule is 13%.⁴⁰ The selective binding of the thiolated protein on the nanowire was then visualized by fluorescent antimouse IgG, which binds selectively to the KE2 antibody.

Figure 4 shows light microscope and fluorescence images for a typical Au/Ni/Au nanowire functionalized by this method. The fluorescence image reveals the nanowire with two bright ends. The fluorescence intensity is proportional to the concentration of protein present on the surface of the nanowire. It is clear from

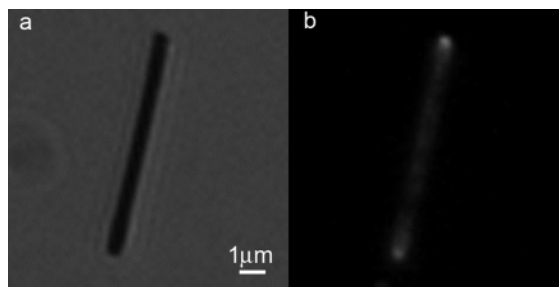


Figure 4. (a) Bright-field and (b) fluorescence images of a Au/Ni/Au nanowire with a KE2 antibody bound to the Au end-segment (Scheme 1).

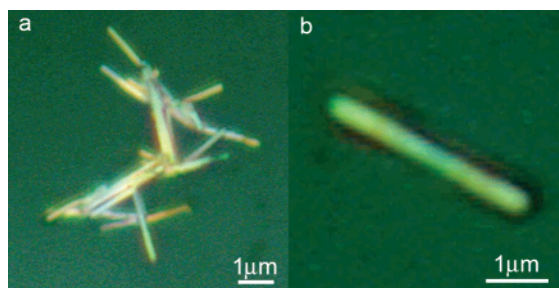


Figure 5. (a) Optical (reflected light) images of a group of Au/Ni nanowires and (b) a single Au/Pt/Au nanowire.

the image that more protein is present at the ends of the wire than in the middle. The fluorescent intensity ratio for the wire in Figure 4 is 3.1, illustrating that the siloxane linkage to the Ni segments is robust and is not displaced by the thiolated protein. In addition, it is clear that the thiol groups on the protein displace any nonspecifically bound siloxane from the Au segments. Furthermore, the PEG-terminated Ni segments show good protein resistance. The number of sulfhydryls per protein can be modified by adjusting the pH (and hence the number of unprotonated amines) and the SATP/protein ratio (in our case the SATP/protein ratio was 68). However, this scheme does not provide control of the location of the sulfhydryls on the protein, which can influence the way in which the protein is bound to the surface as well as the protein activity.

In this example, the protein-resistant segments are Ni. Nanowires with Ni segments tend to exhibit excessive aggregation. A reflected light image of a Au/Ni nanowire aggregate is shown in Figure 5a. This aggregation cannot be ascribed to magnetic interactions because experiments where the nanowires were collected by centrifugation rather than by using a magnet also exhibit aggregation.

In Scheme 2, a protein is bound selectively to the Au end segment of Au/Pt nanowires through a thiol linkage introduced into the protein. The nanowires are first functionalized with butyl isocyanide. The isocyanide group has a strong affinity for the Pt but also binds nonspecifically to the Au segments. The nanowires are then exposed to the thiolated protein, in this case ActA, conjugated with a terminal fluorescein. This protein was also thiolated at pH 7.4. At this pH, the probability of unprotonated α and ϵ amines is similar to that of the IgG molecule since ActA has approximately 40 lysines and a total of 604 residues.

Figure 6 shows light microscope and fluorescence images of a nanowire functionalized according to this scheme. The fluorescence image shows a pronounced difference in intensity between segments, illustrating that the isocyanide was selectively bound to the Pt segment during functionalization with the thiol-modified protein. The fluorescence intensity ratio between the Au and Pt segments is 5.6, indicating that the differential

(39) Wong, S. S. *Chemistry of Protein Conjugation and Cross-linking*; CRC Press: Boca Raton, FL, 1991.

(40) Boyd, W. *Fundamentals of Immunology*, 3rd ed.; Interscience Publishers: New York, 1956.

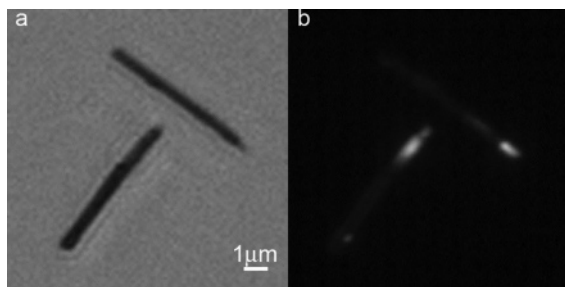


Figure 6. (a) Bright-field and (b) fluorescence images of a Au/Pt nanowire with ActA bound to the Au end-segment (Scheme 2).

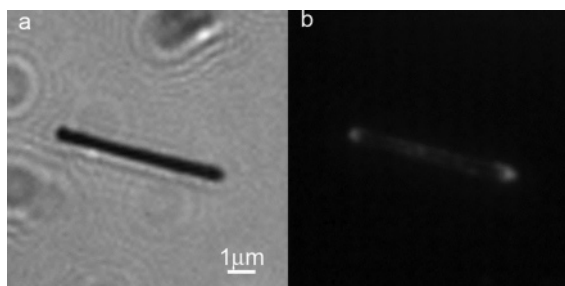


Figure 7. (a) Bright-field and (b) fluorescence images of a Au/Pt/Au nanowire with ActA bound to the Au end-segments (Scheme 3).

functionalization was successful. Improved selectivity could be achieved using a more hydrophilic end-group (e.g., a terminal hydroxyl group) or by introducing PEG groups. Finally, we note that Pt nanowires do not exhibit significant aggregation, a significant advantage compared to Ni nanowires.

Quantitative comparison of the functionalization schemes is complicated by a number of factors. First, the quantum yield is dependent on the protein and fluorophore. Second, fluorescence quenching due to the proximity of the nanowire segment may reduce the quantum yield, and in our experiments, the length of the surface coupling linkage is different in each scheme.

In Scheme 3, the protein ActA was attached to the Au end-segments of Au/Pt/Au nanowires using the succinimide coupling reaction to attach biotin groups to the primary amines on the protein. The Pt segments were first functionalized with butyl isocyanide. The nanowires were then exposed to amine-terminated thiol that was subsequently reacted with a biotin-terminated succinimide with a PEG spacer. Fluorescently labeled avidin was then attached to the biotin on the nanowires. The biotin/avidin linkage has the highest affinity ($K_a = 10^{15} \text{ M}^{-1}$) among biological interactions. NeutraAvidin was chosen specifically in this scheme because it binds at neutral pH which minimizes nonspecific adsorption. The biotinylated protein was then bound to the avidin on the Au end-segments of the nanowire. Figure 5b shows a reflected light image of a Au/Pt nanowire. Figure 7 shows light microscope and fluorescence images for a nanowire functionalized using this scheme. The nanowires showed significant protein asymmetry with a fluorescence intensity ratio of 2.1, which indicates that it is less selective than for the other schemes. Assuming an avidin footprint of 20 nm^2 , we determine that the avidin concentration corresponds to an excess of 470. An excess of avidin is necessary to prevent self-assembly and hence aggregation, which may be detrimental to some biological applications.¹³

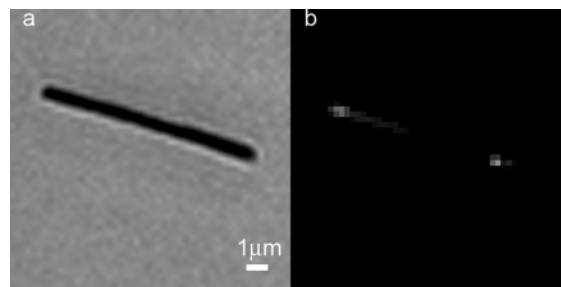


Figure 8. (a) Bright-field and (b) fluorescence images of an Au/Pt nanowire with ActA bound to the Au end-segment (Scheme 4).

Schemes 1–3 involve protein conjugation through primary amines. As discussed above, labeling through unprotonated primary amines does not provide control over where the sequence is altered. Cysteine residues are much less common than lysine residues in most protein sequences, and hence an alternative strategy is to engineer a single cysteine at the end of a protein. ActA has no naturally occurring cysteine residues but can be genetically engineered to contain a cysteine at its C terminus.⁴¹

In Scheme 4, the protein was bound to the nanowire through a biotin–avidin–biotin linkage. This linkage was created by biotinylating the protein through a maleimide coupling group that reacts with sulfhydryl groups present on the terminal cysteine residue. Maleimides react with sulfhydryl groups by forming a thioether linkage at a pH of 6.5 to 7.5. As with NHS, hydrolysis of the maleimide is a competing reaction at pH >8.0. Coupling of the maleimide with primary amines is also a competing reaction at pH >8.5. This approach is shown in Scheme 4. The Au/Pt nanowires were first functionalized with butyl isocyanide, as described in Scheme 2. The nanowires were then exposed to an amine-terminated thiol. The succinimide coupling reaction was then used to attach a biotin group through a PEG spacer in the presence of triethylamine. Triethylamine was added as a base to reduce the number of protonated primary amines during the NHS coupling reaction. A biotin group on the surface of the nanowire is available to bind with avidin. After avidin addition and subsequent washing, biotinylated ActA–Cys was added and bound to avidin. Figure 8 shows light microscope and fluorescence images of a nanowire using this scheme. The fluorescence intensity ratio was 2.4.

In summary, these schemes demonstrate four different methods for selective protein functionalization of multisegment nanowires. Selective protein functionalization is very difficult to achieve because of the adhesive nature of proteins. Here we have demonstrated four differential protein-functionalization strategies that can be adapted to a wide range of proteins and nanowire segments.

Acknowledgment. We thank Zhu Liu for helpful discussions on nanogap fabrication and Chris Merchant for assistance with carbon nanotube synthesis AFM imaging. We thank Mark Koontz assistance with SEM imaging and Dr. Michael Edidin, Dr. Gerald Meyer, and Amanda Fond for helpful discussions on nanowire functionalization. This work was supported by the JHU MRSEC (NSF grant number DMR05-20491) and a graduate fellowship from the Whitaker Foundation.

LA061184J

(41) Upadhyaya, A.; Chabot, J. R.; Andreeva, A.; Samadani, A.; van Oudenaarden, A. *Proc. Natl. Acad. Sci. U.S.A.* **2003**, *100*, 4521–4526.